MINERALOGIA POLONICA
Vol. 35, No 2, 2004
PL ISSN 0032-6267

Krzysztof DUDEK[1], *Krzysztof BUKOWSKI*[1], *Wiesław HEFLIK*[1]

MINERALOGICAL CHARACTERISTICS OF THE BOCHNIA TUFF FROM THE CHODENICE BEDS (CARPATHIAN FOREDEEP, S POLAND)

Abstract. The tuff from the Chodenice Beds, sampled in a natural outcrop in Chodenice, was subjected to mineralogical and geochemical analyses. Main components of the rock proved to be glass shards, quartz and feldspar crystals, as well as mixed-layered Ca-Na-smectite, formed by alteration of volcanic glass. The distinguished heavy fraction consists of ilmenite (predominating component), zircon, secondary iron oxides and scarce crystals (or crushed fragments) of apatite, tourmaline, rutile, monazite, garnet and staurolite. SEM/EDS analyses revealed crypto-inclusions of a metallic, Ni-Fe-rich phase, presumably of cosmic origin.

Key-words: tuff, Chodenice Beds, smectite, zircon, taenite

GEOLOGICAL BACKGROUND

Chodenice, once a village near Bochnia, presently within the borders of the town (Fig. 1), is the type locality for the Chodenice Beds (Niedźwiedzki 1883, *fide* Alexandrowicz 1961). In the general stratigraphic column of Middle Miocene (Badenian) in the Wieliczka-Bochnia area they overlie the evaporites of the Wieliczka Formation and marly and clastic sediments of the Skawina Beds (Fig. 2), all these units belonging to the so-called folded Miocene. The Chodenice Beds, up to 350 metres in thickness, consist of dark-grey or brownish marly clays, fine-grained sandstones and sands, and several intercalations of pyroclastic sediments, mostly in the upper part of the profile (Porębski 1999). The Bochnia Tuff (TB), occurring 200–250 metres above the bottom of the Chodenice Beds, is one of the most broadly extended pyroclastic horizons in the whole Carpathian Foredeep (Alexandrowicz 1997). In the area between Wieliczka and Bochnia it was encountered in several natural outcrops (Chodenice, Chełm upon Raba, Moszczenica, Sułków), in the Bochnia Salt Mine as well as in numerous drillholes. In other parts of the Carpathian Foredeep this horizon was reported from the Upper

[1] AGH, University of Science and Technology, Faculty of Geology, Geophysics and Environment Protection, al. Mickiewicza 30, 30-059 Kraków, Poland; e-mail: kadudek@uci.agh.edu.pl, buk@geolog.geol.agh.edu.pl

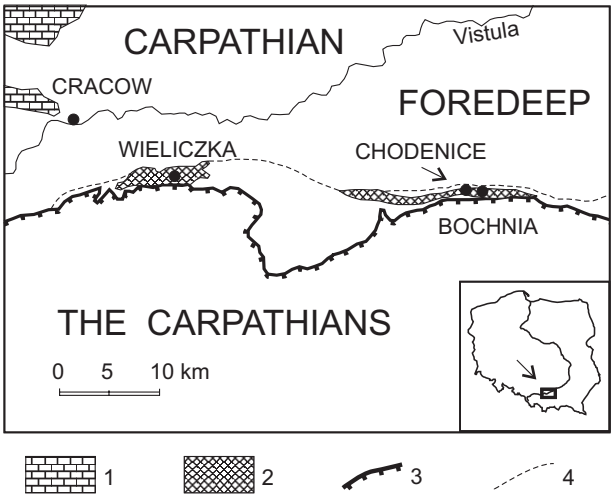

Fig. 1. Geological sketch of the Wieliczka-Bochnia area
1 — platform Mesozoic sediments, 2 — Miocene salt deposits, 3 — Flysch Carpathians border, 4 — extent of folded Miocene sediments

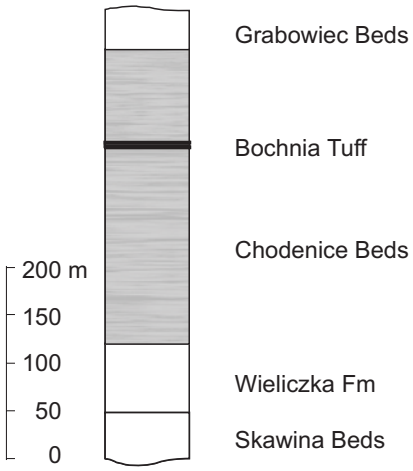

Fig. 2. Position of the Bochnia Tuff and Chodenice Beds in the generalized profile of Middle Miocene (Badenian) for the Wieliczka-Bochnia area

Silesia (Alexandrowicz, Pawlikowski 1980) and from drillholes near Mielec and Przemyśl (Parachoniak 1962).

SAMPLES

A natural outcrop of the Bochnia Tuff, situated on the high, left bank of the Grabowiec creek in Chodenice, was investigated as far as 50 years ago (Parachoniak 1954).

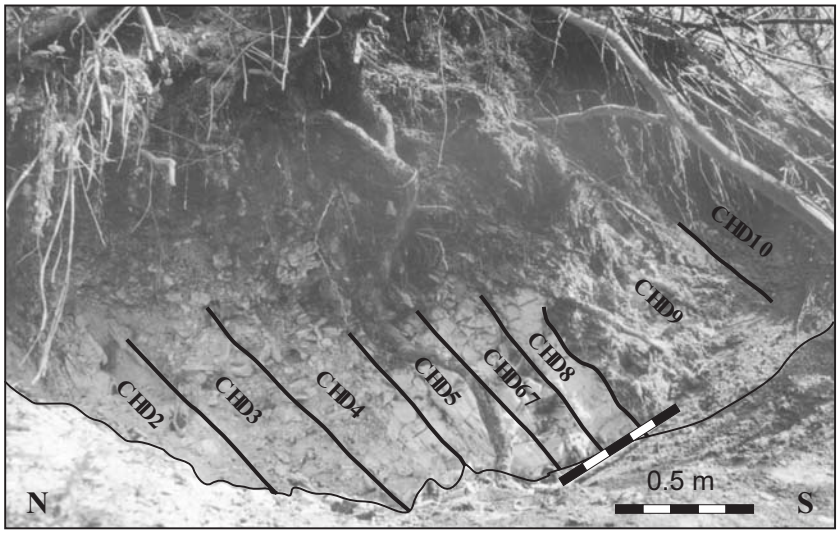

Fig. 3. The investigated outcrop in Chodenice with the distinguished tuff (CHD2–CHD8) and marly (CHD9, CHD10) layers

Presently the outcrop is significantly smaller, not more than three metres in length and around one metre in height (Fig. 3). Field work resulted in distinguishing several layers of pyroclastic sediments (CHD1–CHD8) and two adjacent layers of marly clays (CHD9 and CHD10) at the southern edge of the outcrop, all of them dipping to the south at steep angles of about 60–70°. The layers CHD2, CHD4 and CHD8 represent hell-grey or even whitish, medium-grained tuff, the layers CHD1, CHD3, and CHD67 — fine--grained, and the layer CHD5 — very fine-grained material. The layers of coarser (medium-grained) tuff are somewhat thicker (up to 30 cm), devoid of lamination, and easily weather into loose debris and mineral grains. The fine-grained varieties are slightly darker and distinctly laminated, splitting into thin, relatively hard plates. All the layers distinguished were sampled for laboratory analyses.

METHODS

Samples of the tuff and adjacent marls were subjected to microscope observations in thin sections. Then, clay and heavy fractions were separated. The distinguished heavy fractions as well as coarser grains were examined under a binocular microscope, heavy minerals having been determined in grain mounts with a polarizing microscope. Polished thin sections and selected grains of main and accessory minerals were observed and analysed with the SEM/EDS apparatus.

Clay fractions (below 2 μm) were separated from coarser components of mechanically disintegrated rocks as relevant-size particles suspended in distilled water, thereafter sedimented and dried in evaporating dishes. Samples prepared in this way were subjected to X-ray powder diffraction, IR spectroscopy, DTA, SEM/EDS analyses,

and ICP chemical analyses for major and trace elements. ICP chemical analyses were also carried out for selected whole-rock samples.

Microscope observations were made with the Olympus BJ51 polarizing microscope, microphotographs were taken with a digital camera and processed with the AnalySIS computer program. Heavy minerals were separated in tetrabromoethane ($C_2H_2Br_4$, d = 2.97 $g \cdot cm^{-3}$) from the coarser grain fractions (> 0.0625 mm) of disintegrated samples.

X-ray analyses were made with a Philips X'pert APD PW 3020 diffractometer, using CuK_α radiation, and a graphite reflexion monochromator. The clay fractions were analysed in the form of powdered samples with randomly oriented grains as well as parallel oriented grains, sedimented from suspension on glass slides. The latter were also analysed after saturation with ethylene glycol and after heating to 500°C.

IR spectra were registered with a Bio-Rad FTS 165 Fourier Transform Infrared spectrometer. The clay fractions were prepared in the form of discs (1 mg of a sample pressed with 300 mg KBr) and self-supporting films, produced on Mylar foil, from several drops of a clay sample, earlier dispersed in distilled water with an ultrasonic disintegrator. After evaporation of water at a room temperature, thin layers of dried clay were separated out of the Mylar substratum. Self-supporting smectite films were placed in a FTIR gas cell, the spectra were registered during 60 seconds.

Differential thermal analysis was made with a Hungarian MOM Derivatograph-C; samples weighting 200 mg were heated in the temperature range 20–1000°C.

SEM/EDS analyses were made in the FESEM Laboratory of the Institute of Geological Sciences, Jagiellonian University, using a NORAN Vantage spectrometer coupled to a HITACHI S-4700 scanning electron microscope operating at 15 kV. Chemical analyses with the ICP method were made by the Activation Laboratory, Ancaster, Canada.

RESULTS

Microscope analysis revealed that the non-laminated, medium-grained tuff is composed of glass shards, crystals, and sparse rock fragments disseminated in clay matrix (Phot. 1). The main component of the clay matrix, displaying dark-brownish interference colours, is apparently smectite formed through alteration of the volcanic glass. The pumice- and obsidian-type shards are of dimensions of tiny ash and volcanic dust, generally below 0.2 mm. The obsidian shards often display characteristic parallel cleavage and fan-like bending. Feldspars and quartz, prevailing among the crystal components of the tuff analysed, usually occur as euhedral or subhedral tablets (feldspars) or sharp-edged, wedge-shaped broken fragments (quartz), up to 0.3–0.5 mm. The feldspars are sanidine, Na-Ca plagioclases as well as high-temperature anorthoclase, relatively rich in both Na and K (Table 1). Observations of disintegrated rock under binocular microscope revealed octahedral crystals of pyrogenic quartz, up to 0.5 mm (Phot. 2). Less frequent crystal components are colourless flakes of muscovite and/or hydromuscovite, and pale-brown ones of weathered biotite, with adjacent aggregates

TABLE 1

EDS analyses of glass, feldspars and biotite from medium-grained tuff, sample CHD8. Total iron as Fe_2O_3 in glass and feldspars, as FeO in biotite. Cations normalized to 24 oxygens in glass and feldspars and to 22 oxygens in biotite

Component	Glass 87-6-1	Feldspar 87-2-1	Feldspar 87-4-7	Biotite 8H-28-1	Biotite 8H-28-2	Biotite 8H-28-3
SiO_2	80.34	78.71	80.78	30.49	32.32	31.28
TiO_2				6.52	6.05	6.22
Al_2O_3	12.15	11.50	12.10	11.75	12.65	12.11
Fe_2O_3/FeO	1.63	3.45	1.50	36.81	34.58	35.65
MgO		0.35		4.05	4.54	4.41
CaO	0.98	1.18	0.78			
CuO				1.02	0.86	1.26
K_2O	2.89	3.13	2.85	9.01	8.75	8.87
Na_2O	2.01	1.46	1.99			
Cl		0.22		0.35	0.25	0.20
Total	**100.00**	**100.00**	**100.00**	**100.00**	**100.00**	**100.00**
Cations						
Si	10.211	10.110	10.247	5.425	5.620	5.507
Ti				0.872	0.791	0.823
Al	1.820	1.741	1.808	2.464	2.592	2.513
Fe	0.156	0.334	0.143	5.477	5.028	5.250
Mg		0.067		1.075	1.178	1.156
Ca	0.133	0.162	0.106			
Cu				0.137	0.114	0.168
K	0.468	0.513	0.461	2.045	1.940	1.992
Na	0.496	0.364	0.488			
Total	**13.284**	**13.291**	**13.253**	**17.495**	**17.263**	**17.409**

of dark-brown or opaque iron oxides. Accessory components are sparsely distributed green aggregates of glauconite and isometric, opaque crystals of ilmenite, in thin sections below 0.1 mm. Transparent heavy minerals are very rare and in thin sections practically indistinguishable.

Fine-grained tuff varieties, displaying distinct lamination on microscopic scale, are mostly composed of clay matrix and glass shards. Minor components are tiny flakes of micas and sparse, isolated crystals of quartz and feldspars, less abundant and smaller (0.1–0.2 mm) than in the medium-grained tuff.

The adjacent marls are yellow-brown, soft and plastic, with weak (CHD9) and more intensive (CHD10) reaction with diluted HCl. The sample CHD9 consists of clay minerals with sparse, tiny quartz grains (below 0.1 mm) and flakes of hydromuscovite. The second layer (CHD10) is mostly composed of microcrystalline carbonate mineral (proved to be dolomite in the X-ray analysis) with pale interference colours. Minor components are sharp-edged quartz grains, iron-oxide aggregates and bioclasts in the form of shell fragments.

The clay particles (below 2 μm), ubiquitous in all the tuff and marl samples examined, were analysed after having been separated from coarser components. The distinguished clay fraction accounts for 10–12 wt.% of the fine-grained tuff samples (CHD5, CHD67), but only for 2–3 wt.% of the medium-grained ones (CHD1, CHD2, CHD4, CHD8). X-ray diffraction patterns of clay samples demonstrate that the predominating component in all of them is smectite, with the main peak (d_{001}) at 15.44–15.73 Å in cases of randomly arranged crystals, and at 14.44–15.35 Å for oriented samples (Table 2). These differences may result from varying contents of interlayer water molecules, caused by drying of the material analysed. For the oriented samples the d_{001} peak was shifted to 17.17–17.51 Å after treatment with ethylene glycol, and to 9.82–10.05 Å after heating to 500°C. The X-ray patterns represent practically pure, swelling smectite with small admixture of quartz, indicated by a very weak peak at 4.27 Å (Fig. 4).

TABLE 2

Values of the first-order peak (d_{001}, in Å) in the clay fraction samples distinguished from the analysed tuff

Sample	Random	Oriented	Glycolated	Heated
CHD2cl	15.73	14.44	17.20	10.05
CHD4cl	15.51	15.02	17.51	10.04
CHD5cl	15.44	15.35	17.27	10.02
CHD8cl	15.56	14.99	17.17	9.82

The IR spectra of the clay samples were identified with help of widely known published data (Moenke 1962; Van der Marel, Beutelspacher 1976); the registered absorption bands are listed in Table 3. The spectra of samples dispersed in KBr discs display strong maxima at 470, 525 and 1057 cm^{-1}, related to Si-O and Al-O structural stretching vibrations in tetrahedral layers, and several weak ones in the range 600–940 cm^{-1}. Distinct absorption bands at 1635 and 3400 cm^{-1} indicate the presence of H_2O molecules, whereas a sharp maximum around 3620 cm^{-1} is due to stretching vibrations of the OH groups (Fig. 5). In the self-supporting film spectra the 470, 525 and 1057 cm^{-1} peaks are extremely high, but the remaining ones appear more distinct, enabling their precise determination (Table 3, Fig. 6). The maximum at 800 cm^{-1}, together with slight inflexion of the spectrum around 780 cm^{-1} apparently mark a small admixture of quartz pelite. The absorption bands at 840 and 917 cm^{-1} are related to Mg-OH and Al-OH

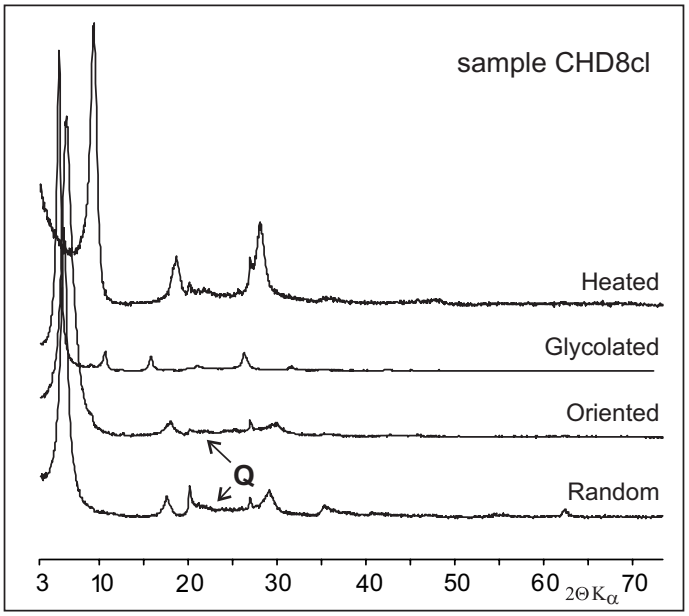

Fig. 4. X-ray patterns of clay fraction (sample CHD8cl) separated from medium-grained tuff

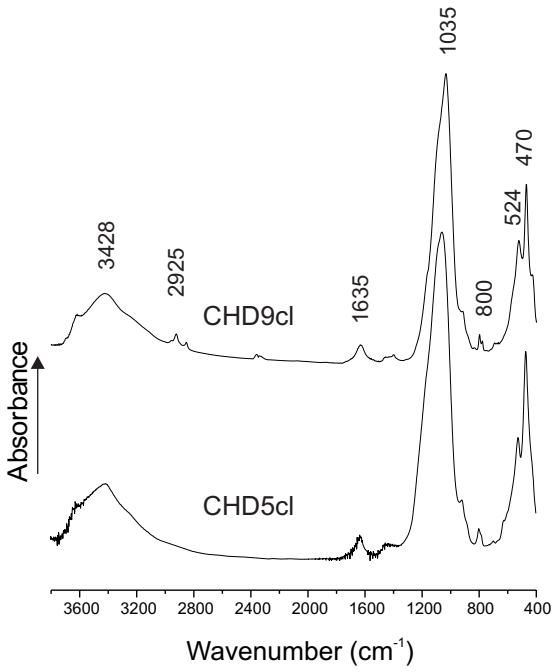

Fig. 5. IR spectra of clay fractions — samples CHD5cl and CHD9cl in KBr discs

TABLE 3

Absorption peaks (in cm^{-1}) in the IR spectra of the clay fractions; information on sample preparation (KBr discs or self-supporting films) in brackets

CHD5cl (KBr)	CHD5cl (film)	CHD67cl (film)	CHD8cl (film)	CHD4cl (film)	CHD2cl (film)	CHD9cl (KBr)	CHD9cl (film)
	405			405	420	431	
470						471	
525						524	
				627			
		692					780
799	800	799	799	800	800	800	800
	844	838	843	844	840		837
911	917	917	917	915	916	911	917
1 057						1 035	
1 630	1 635	1 635	1 635	1 635	1 634	1 635	1 635
3 413	3 400	3 400	3 400	3 400	3 400	3 428	3 400
3 629	3 625	3 622	3 622	3 622	3 622		3 622

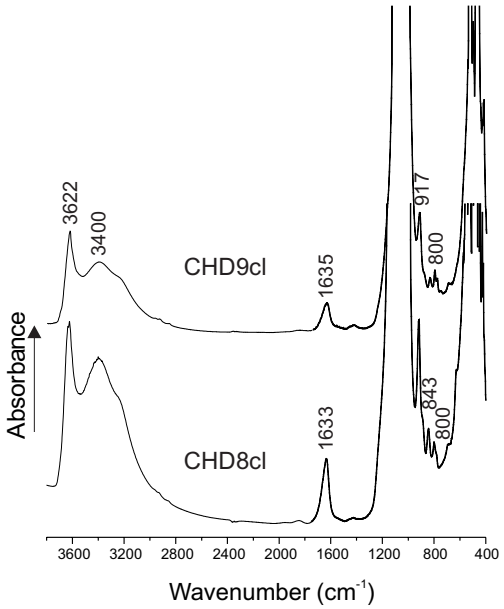

Fig. 6. IR spectra of clay fraction — samples CHD8cl and CHD9cl as self-supporting films

deformation vibrations in octahedral layers. The above listed H_2O and OH vibrations could be precisely ascertained to 1635 (H_2O bending vibrations), 3400, and 3622–3625 cm^{-1}. The whole IR absorption spectra of selected samples are presented in Figs 5 and 6.

DTA patterns of three clay samples analysed indicate strong endogenic effects around 140°C, accompanied by 9% of loss on weight in the temperature range 20–200°C, related to physically adsorbed and interlayer water. Lower, though systematic loss on weight of 4.0–4.5% was registered in the TG curves in the range 200–700°C. Small endogenic effects on the DTA curve around 540 and 685°C are related to dehydroxylation of illite and pure montmorillonite layers, respectively (Wyrwicki 1988). Total loss on weight amounts to 12% in the case of the clay fraction from the CHD9 marl sample and to around 14–15% for the clays from the tuff samples (Fig. 7).

Chemical analyses of clay samples, performed with the ICP method, are presented in Table 4. Normalization of the oxide contents led to a general formula:

$$K_{0.11}Na_{0.04}Ca_{0.09}Mg_{0.23}Fe_{0.16}Al_{1.22}Si_{4.30}O_{10}(OH)_2 \cdot 2.3H_2O$$

Such results indicate a certain excess of SiO_2, accompanied by a deficit of exchangeable cations (K, Na and Ca). The excess of silica is presumably due to admixtures of quartz pelite and acid, silica-rich volcanic glass, whereas the cations could have been partly removed during separating of clay fractions from coarser particles in distilled

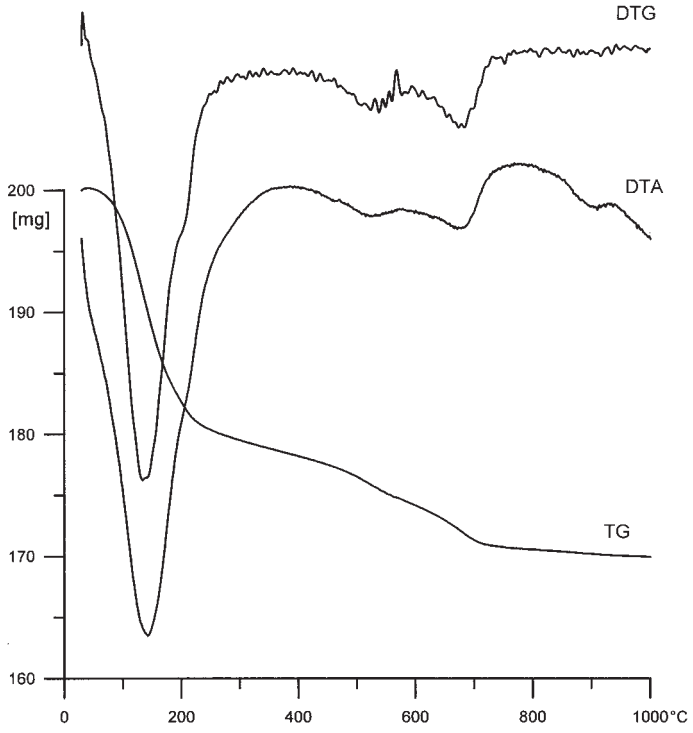

Fig. 7. DTA, DTG and TG curves for clay fraction — sample CHD5cl

TABLE 4

ICP chemical analyses of clay fractions distinguished from the analysed tuff samples.
Total iron as Fe_2O_3, cation contents normalized to 11 oxygens

Component \ Sample	CHD5cl	CHD8cl	CHD67cl	CHD9cl
SiO_2	62.39	55.35	63.50	54.35
Al_2O_3	15.09	16.71	13.99	16.10
Fe_2O_3	3.01	4.31	3.09	7.90
MnO	0.03	0.01	0.01	0.04
MgO	2.21	2.59	2.04	2.45
CaO	1.04	1.51	1.23	1.28
Na_2O	0.34	0.27	0.32	0.26
K_2O	1.31	0.72	1.50	2.68
TiO_2	0.25	0.21	0.28	0.51
P_2O_5	0.04	0.13	0.05	0.22
LOI	14.45	18.39	14.07	14.25
Total	**100.16**	**100.20**	**100.08**	**100.04**
Cations				
Si	4.27	4.01	4.33	3.88
Al	1.22	1.43	1.12	1.35
Fe	0.15	0.24	0.16	0.42
Mn	0.00	0.00	0.00	0.00
Mg	0.23	0.28	0.21	0.26
Ca	0.08	0.12	0.09	0.10
Na	0.05	0.04	0.04	0.04
K	0.11	0.07	0.13	0.24
Ti	0.01	0.01	0.01	0.03
P	0.00	0.01	0.00	0.01
Total	**6.12**	**6.21**	**6.09**	**6.33**

water. Loss on weight of around 15 wt.%, in perfect agreement with the DTA results, accounts for two OH groups and 2.3 H_2O molecules pfu. The EDS data, regardless of non registered water content, indicate similar proportions of major oxides and cations as the chemical analyses.

Accessory heavy minerals proved to be more abundant in the medium-grained tuff layers (CHD2, CHD4, and CHD8) than in the fine-grained ones (CHD5 and CHD67).

The predominating component of the heavy fraction is ilmenite, occurring in form of black, rhombohedral tablets, the largest reaching 0.3 mm (Phot. 3), but most of them being below 0.1 mm. The ilmenite crystals contain small admixtures of MgO, MnO (each around 1.5 wt.%), and V_2O_5 (below 0.8 wt.% — see Table 5). Other opaque

TABLE 5

EDS chemical analyses of heavy minerals from sample CHD8. Total iron as Fe_2O_3 in tourmaline and as FeO in staurolite, garnet, and ilmenite analyses. Cation contents normalized to 24 oxygen atoms

Sample / Component	Tourmaline 8H-11-1	Tourmaline 8H-17-1	Tourmaline 8H-23-1	Staurolite 8H-25-1	Garnet 8H-32-1	Ilmenite 8H-1-1	Ilmenite 8H-4-3
SiO_2	43.47	43.93	42.85	26.31	34.71		
TiO_2	0.73	0.82	0.82	0.91	0.23	48.11	48.38
Al_2O_3	34.05	38.34	34.57	52.12	18.97	0.42	
Fe_2O_3/FeO	7.60	3.77	7.90	16.99	25.98	47.66	48.28
V_2O_5						0.71	0.49
MgO	8.99	8.99	8.20	1.03	1.52	1.76	1.44
MnO				0.84	16.08	1.34	1.41
CaO	0.56	1.02	0.51		1.15		
Na_2O	2.81	2.09	2.93				
CuO	0.98	1.04	1.16	1.80	1.36		
ZnO	0.81		1.06				
Total	**100.00**	**100.00**	**100.00**	**100.00**	**100.00**	**100.00**	**100.00**
Cations							
Si	5.965	5.909	5.903	3.852	5.817		
Ti	0.075	0.083	0.085	0.101	0.030	7.365	7.445
Al	5.507	6.077	5.612	8.992	3.748	0.101	
Fe	0.785	0.381	0.818	2.081	3.642	8.115	8.261
V						0.096	0.066
Mg	1.840	1.802	1.684	0.224	0.380	0.534	0.440
Mn				0.104	2.284	0.230	0.244
Ca	0.083	0.147	0.075		0.207		
Na	0.749	0.546	0.783				
Cu	0.102	0.106	0.121	0.199	0.172		
Zn	0.082		0.108				
Total	**15.188**	**15.051**	**15.189**	**15.553**	**16.280**	**16.441**	**16.456**

components of the heavy fraction are dark-brownish, relatively loose and porous aggregates of secondary iron oxides.

Microscope inspection of grain mounts enabled to identify such transparent minerals as zircon, apatite, tourmaline, rutile, monazite, garnet, staurolite, and biotite. Zircon crystals generally occur as euhedral, elongated prisms up to 0.2 mm in length (Phot. 4), while small (0.05 mm), rounded grains (Phot. 5) are significantly less frequent. Most of the analysed zircons are pure $ZrSiO_4$, only some of the euhedral crystals contain small amounts of HfO_2, up to 2.22 wt.%, i.e. less than 0.02 Hf pfu. Apatite was observed in form of euhedral prisms (Phot. 6), chemically pure. Tourmaline, staurolite, garnet and rutile were observed only as sharp-edged fragments of broken crystals; chemical analyses are presented in Table 5. Monazite, observed only in few grains, displays numerous isomorphic admixtures of REE (Table 6). SEM/EDS analyses of a polished thin section allowed detecting submicroscopic inclusions of Ni-Fe rich phases (Phot. 7). The chemical analyse indicates 95.60% Ni, 2.75% Fe, and 1.65% Si (in wt.%), the last value could have been from the surrounding silicate. Such a Ni/Fe ratio indicates Ni-rich taenite.

TABLE 6

EDS chemical analysis of monazite from sample CHD8 (8H-21-1). Cation contents normalized to 24 oxygen atoms

Component	SiO_2	P_2O_5	ThO_2	CaO	La_2O_3	Ce_2O_3	Nd_2O_3	Sm_2O_3	Gd_2O_3	Pr_2O_3	Total
Oxide content [wt.%]	0.31	36.17	6.01	2.25	10.18	27.94	10.09	2.40	1.16	3.49	100.00
Cation	0.066	6.537	0.292	0.515	0.802	2.184	0.769	0.176	0.082	0.272	11.695

Chemical analyses of whole-rock samples are presented in Table 6. High content of silica (over 70 wt.%) and relatively high amounts of alkalis (over 2.0% Na_2O and over 2.5% K_2O) indicate acid composition of the analysed tuff from Chodenice.

CONCLUDING REMARKS

Mineral and chemical composition of the investigated tuff samples indicate strongly acid character of the parent material. Abundant pyrogenic components, like glass shards, high-temperature alkali feldspars, euhedral, pseudo-hexagonal biotite flakes, and bipyramidal quartz, record its volcanic origin (Fisher, Schmincke 1984). This is also supported by mineral composition of the heavy fractions and euhedral shapes of predominating components (ilmenite, zircon). On the other hand, an admixture of rounded grains of zircon and broken fragments of metamorphic minerals (garnet, staurolite) indicate more complex origin of the sediments analysed. Crypto-inclusions

TABLE 7

Chemical analyses of whole-rock samples of the tuff from Chodenice

Component \ Sample	CHD2r	CHD5r	CGD67r	CHD8r
SiO_2	75.89	70.78	70.55	70.35
Al_2O_3	10.55	12.30	12.46	12.71
Fe_2O_3	1.54	1.63	1.59	1.39
MnO	0.032	0.029	0.026	0.031
MgO	0.36	0.63	0.69	0.53
CaO	0.94	1.01	1.04	1.19
Na_2O	2.31	2.18	2.03	2.62
K_2O	2.52	2.71	2.61	2.64
TiO_2	0.167	0.149	0.133	0.156
P_2O_5	0.04	0.03	0.03	0.04
LOI	5.71	8.13	8.59	7.93
Total	100.06	99.58	99.75	99.59

of a metallic, Ni-Fe-rich phase, presumably of cosmic origin, record a fall of extra--terrestrial matter during the sediment formation. Ubiquitous smectite, practically of the same composition in subsequent tuff layers, points out to advanced alteration of the volcanic glass in rather uniform, sub-marine conditions.

Sequence of the distinguished tuff layers, granularity, size distribution and other textural features indicate that the whole series analysed represents at least three subsequent volcanic events. Direct contact of the medium-grained tuff with the overlying marly clays demonstrates that the whole complex in the area of the discussed outcrop in Chodenice is reversed (Parachoniak 1954; Dudek, Bukowski 2002). Small and relatively uniform dimensions of the sediment components suggest rather a distant eruption source, apparently in the neighbouring Carpathians. As published radiometric datings of zircon and biotite from the Bochnia Tuff from Chodenice give the ages slightly over 12 Ma (Van Couvering et al. 1981; Wieser et al. 2000), these pyroclastic sediments could be related to the Carpathian post-orogenic volcanism.

Acknowledgement. This study was financially supported by the Polish Committee for Scientific Research (KBN), grant no 6 PO4 D 089 21.

REFERENCES

ALEXANDROWICZ S.W., 1961: Stratygrafia warstw chodenickich i grabowieckich w Chełmie nad Rabą. *Kwart. Geol.* 5, 3, 646–668.

ALEXANDROWICZ S.W., PAWLIKOWSKI M., 1980: Policykliczny poziom tufitowy w miocenie okolic Gliwic. *Kwart. Geol.* 24, 663–678.

ALEXANDROWICZ S.W., 1997: Lithostratigraphy of the Miocene deposits in the Gliwice area (Upper Silesia, Poland). *Bul. Pol. Acad. Sc., Earth Sc.* 45, 168–179.

DUDEK K., BUKOWSKI K., 2002: New data on the Bochnia tuff from Chodenice, Forecarpathians, Poland. *Pol. Tow. Mineral. Prace Spec.* 20, 85–87.

FISHER R.V., SCHMINCKE H.-U. 1984: Pyroclastic Rocks. Springer, Berlin.

MOENKE H., 1962: Mineralspektren. Akademie Verlag, Berlin.

PARACHONIAK W., 1954: Tortońska facja tufitowa między Bochnią a Tarnowem. *Acta Geol. Pol.* 4, 67–92.

PARACHONIAK W., 1962: Mioceńskie utwory piroklastyczne przedgórza Karpat Polskich. *Pr. Geol. Kom. Nauk. Geol. PAN Oddz. w Krakowie*. 11, 7–77.

PARACHONIAK W., PAWLIKOWSKI M., 1980: Hornblenda z tufitu andezytowego z Wieliczki. *Spraw. z Pos. Kom. Nauk. PAN Oddz. w Krakowie*. 21, 2, 127–128.

PORĘBSKI S.J., 1999: Środowisko depozycyjne sukcesji nadewaporatowej (górny baden) w rejonie Kraków–Brzesko (zapadlisko przedkarpackie). *Prace PIG* 168, 97–119.

VAN COUVERING I.A., AUBRY M.P., BERGGREN Q.A., BUJAK J.P., NAESER C., WIESER T., 1981: Terminal Eocene event and Polish connections. *Palaeogeography. Palaeoclimatology, Palaeoecology* 36, 321–362.

VAN DER MAREL H.W., BEUTELSPACHER H., 1976: Atlas of infrared spectroscopy of clay minerals and their admixtures. Elsevier, Amsterdam.

WIESER T., BUKOWSKI K., WÓJTOWICZ A., 2000: Korelacja mineralogiczna i wiek radiometryczny tufitu z warstw chodenickich z okolic Bochni. *V Ogólnopolska Sesja Naukowa: Datowanie Minerałów i Skał, Kraków, 11.02.2000*. 50–55.

WYRWICKI R., 1988: Analiza derywatograficzna skał ilastych. Wyd. UW, Warszawa.

Krzysztof DUDEK, Krzysztof BUKOWSKI, Wiesław HEFLIK

CHARAKTERYSTYKA MINERALOGICZNA TUFITU Z BOCHNI Z WARSTW CHODENICKICH (ZAPADLISKO PRZEDKARPACKIE, S POLAND)

Streszczenie

Analizom mineralogicznym i chemicznym poddano próbki tufitu z Bochni (TB), pobrane z naturalnego odsłonięcia w Chodenicach. Główne składniki tej skały to okruchy szkliwa wulkanicznego, krystaloklasty kwarcu i skaleni oraz mieszanopakietowy Ca-Na-smektyt, będący produktem wietrzenia szkliwa. Wydzielone frakcje ilaste poddano analizie dyfraktometrycznej (wraz z glikolowaniem i prażeniem preparatów orientowanych), spektroskopii absorpcyjnej w podczerwieni, termicznej analizie

różnicowej, mikroskopii elektronowej (wraz z analizą EDS) oraz analizie chemicznej metodą ICP. W wydzielonej frakcji ciężkiej zidentyfikowano ilmenit (główny składnik), cyrkon, wtórne agregaty wodorotlenków żelaza oraz pojedyncze kryształy (lub ich pokruszone fragmenty) apatytu, turmalinu, rutylu, monacytu, granatu i staurolitu. Analizy SEM/EDS ujawniły krypto-inkluzje metalicznej fazy niklowo-żelazowej, zapewne pochodzenia pozaziemskiego.

Uziarnienie i inne cechy teksturalne analizowanego osadu świadczą o stosunkowo dalekim transporcie drobnego materiału wulkanicznego, zapewne z sąsiednich Karpat. Skład mineralny i chemiczny skał oraz publikowane wyniki datowań radiometrycznych wskazują, że analizowany osad piroklastyczny jest zapewne produktem kwaśnego wulkanizmu postorogenicznego.

a)

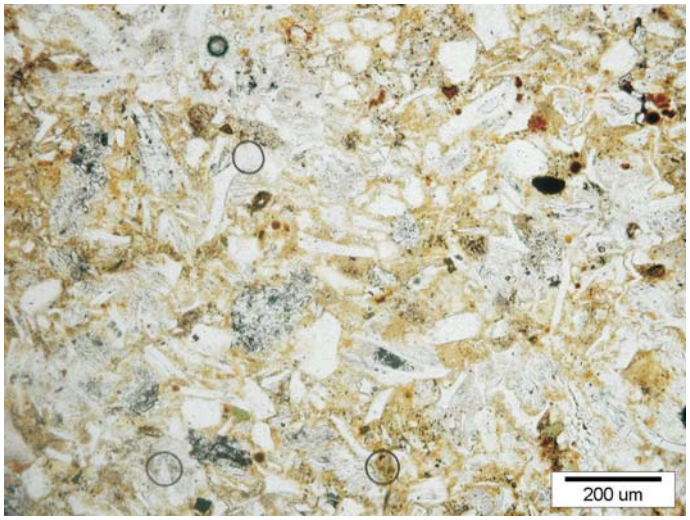

b)

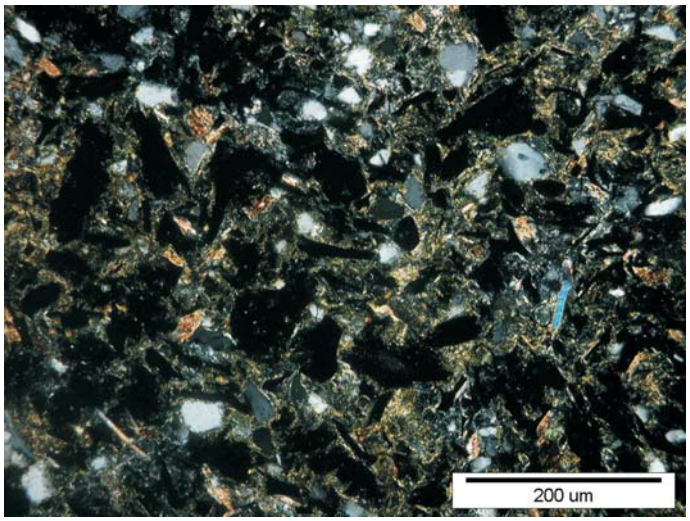

Phot. 1. Microphotograph of medium-grained tuff (sample CHD8)
a — plane polarized light; b — crossed polars

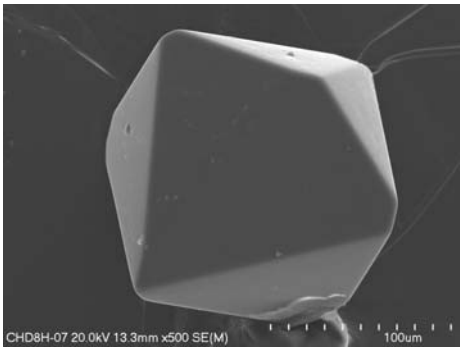

Phot. 2. SEM image of bipyramidal quartz

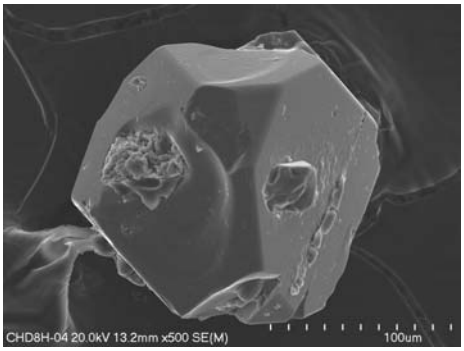

Phot. 3. SEM image of ilmenite euhedral crystal with included apatite (right from the centre)

Phot. 4. SEM image of zircon euhedral crystal with apatite overgrown (in lower part of the zircon prism)

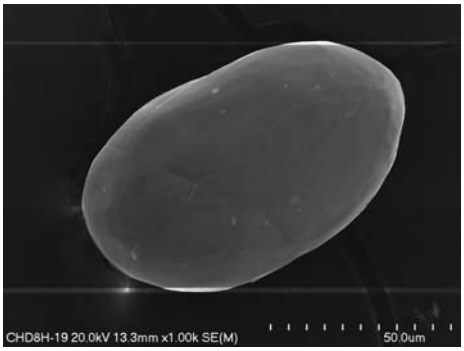

Phot. 5. SEM image of rounded zircon grain

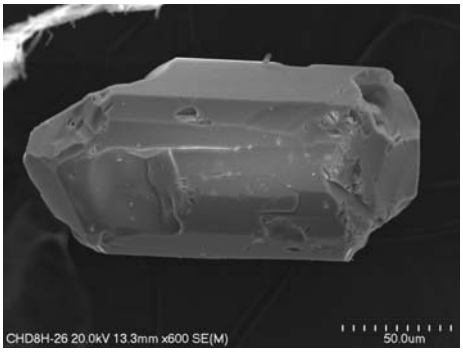

Phot. 6. SEM image of apatite broken crystal

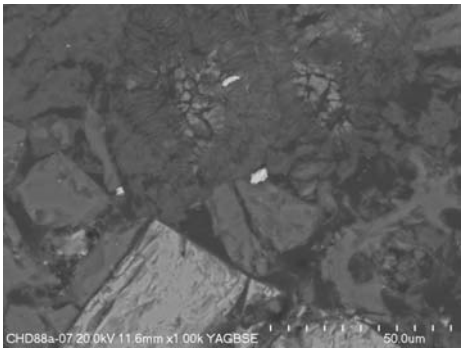

Phot. 7. SEM image of metallic Ni-Fe phases (white spots in the centre)